

Article

Photocatalytic Dye Degradation and Biological Activities of Cu-Doped ZnSe Nanoparticles and Their Insights

V. Beena¹, S. L. Rayar², S. Ajitha¹, Awais Ahmad^{3,*} , Faiza Jan Iftikhar⁴, Khamael M. Abualnaja⁵, Taghrid S. Alomar^{6,*}, Mohmed Ouladsmne⁷  and Shafaqat Ali^{8,9,*} 

¹ Department of Physics, Nanjil Catholic College of Arts and Science, Manonmaniam Sundaranar University, Kanyakumari 629153, India; drbeenaphysics@gmail.com (V.B.); ajithaphyholly@gmail.com (S.A.)

² Department of Physics, St. Judes College, Kanyakumari 629176, India; drslrayar@gmail.com

³ Departamento de Quimica Organica, Universidad de Cordoba, Edificio Marie Curie (C-3), Ctra Nnal IV-A, Km 396, E14014 Cordoba, Spain

⁴ School of Applied Sciences & Humanity, NUSASH, National University of Technology, Islamabad 42000, Pakistan; faizajiftikhar@nutech.edu.pk

⁵ Department of Chemistry, College of Science, Taif University, Taif 21944, Saudi Arabia; k.ala@tu.edu.sa

⁶ Department of Chemistry, College of Science, Princess Nourah bint Abdulrahman University, Riyadh 11671, Saudi Arabia

⁷ Advanced Materials Research Chair, Chemistry Department, College of Science, King Saud University, Riyadh 11451, Saudi Arabia; mouladsmne@ksu.edu.sa

⁸ Department of Environmental Sciences and Engineering, Government College University Faisalabad, Faisalabad 38000, Pakistan

⁹ Department of Biological Sciences and Technology, China Medical University, Taichung 40402, Taiwan

* Correspondence: awaisahmed@gcuf.edu.pk (A.A.); tsalmoar@pnu.edu.sa (T.S.A.); shafaqataligill@yahoo.com (S.A.)



Citation: Beena, V.; Rayar, S.L.; Ajitha, S.; Ahmad, A.; Iftikhar, F.J.; Abualnaja, K.M.; Alomar, T.S.; Ouladsmne, M.; Ali, S. Photocatalytic Dye Degradation and Biological Activities of Cu-Doped ZnSe Nanoparticles and Their Insights. *Water* **2021**, *13*, 2561. <https://doi.org/10.3390/w13182561>

Academic Editor: Stefanos Giannakis

Received: 18 August 2021

Accepted: 7 September 2021

Published: 17 September 2021

Publisher's Note: MDPI stays neutral with regard to jurisdictional claims in published maps and institutional affiliations.



Copyright: © 2021 by the authors. Licensee MDPI, Basel, Switzerland. This article is an open access article distributed under the terms and conditions of the Creative Commons Attribution (CC BY) license (<https://creativecommons.org/licenses/by/4.0/>).

Abstract: Environmental nanotechnology has received much attention owing to its implications on environmental ecosystem, and thus is promising for the elimination of toxic elements from the aquatic surface. This work focuses on Cu-doped ZnSe nanoparticles using the co-precipitation method. The synthesized Cu-doped ZnSe nanoparticles were examined for structural, optical, and morphological properties with the help of XRD, FTIR, UV/vis diffuse reflection spectroscopy (DRS), FESEM, TEM, and XPS. The synthesized Cu-doped ZnSe nanoparticles revealed the presence of Cu²⁺ in the ZnSe lattice, which has been shown to take a predominant role for enhanced catalysis in the Cu-doped ZnSe nanoparticles. The synthesized Cu-doped ZnSe nanoparticles were investigated for their catalytic and antibacterial activities. The 0.1 M copper-doped ZnSe nanoparticles exhibited the highest rate of degradation against the methyl orange dye, which was found to be 87%. A pseudo-first-order kinetics was followed by Cu-doped ZnSe nanoparticles with a rate constant of 0.1334 min⁻¹. The gram-positive and gram-negative bacteria were used for investigating the anti-bacterial activity of the Cu-doped ZnSe nanoparticles. The Cu-doped ZnSe nanoparticles exhibited enhanced photocatalytic and antibacterial activity.

Keywords: Cu-doped ZnSe NPs; MO; photocatalysis; visible light

1. Introduction

For the removal of dyes as organic contaminants in an aqueous system, conventional methods have been in vogue, which include ultrafiltration, reverse osmosis, ion exchange, adsorption, photocatalytic degradation, and so on; nevertheless, these methods cannot completely degrade the organic pollutants [1–7].

Researchers have taken an immense interest in employing nanoparticles for photocatalytic dye degradation. The photocatalytic degradation process [8,9] is a highly efficient oxidation method for decomposing organic contaminants. The electrons are excited and steered from the valence band to the conduction band of the photocatalyst using energy

from an optical source, and highly reactive hydroxyl radicals are generated for oxidation and degradation of contaminants [10]. Thanks to their superior thermal stability, corrosion resistance, and high surface area to volume ratio, metal oxides like titanium oxide, zinc oxide, manganese oxide, and manganese dioxide have gained significant attention for photocatalysis [11]. These materials have been proven to be able to remove a wide spectrum of dyes from the aqueous solutions [12].

Photocatalytic degradation is the most promising technology for removing dyes, pigments, or colorants from aqueous media owing to its efficiency, cost-effectiveness, selectivity, and flexible operation modes. For this purpose ZnSe, an intrinsic semiconductor that absorbs ultraviolet/visible light, has been investigated, having a bandgap of 2.7 eV [13,14]. It is also a strong competitor to other materials for photocatalytic applications owing to its excellent energy band location. ZnSe-based nanostructures, such as ZnO/ZnSe [13,15], Bi₂S₃-ZnSe [14], and FeSe₂/ZnSe [16,17], demonstrate improved photocatalytic performance. Similarly, it is reported that composited polymers act as an active support for nanoparticles for photocatalysis, providing mechanical strength and architectural diversity. PANI/ZnO nanocomposites have been reported for photocatalytic degradation of dyes malachite green and methylene blue under UV and natural sunlight irradiation with 99% efficiency. The presence of Cu-doped ZnSe in the composite polymer films is confirmed by XPS, UV-Vis, and fluorescence studies by [18]. Similarly, different methods have been employed such as the wet chemical approach to successfully manufacture ZnS and metal (Mn, Cu)-doped ZnS. The chemical bonding and crystal structure have been examined using FTIR and X-ray diffraction [19]. Cu-doped ZnS nanoparticles were prepared using a co-precipitation technique and studied via X-ray diffraction (XRD), scanning electron microscopy (SEM), UV-vis absorption spectroscopy, and photoconductivity (PC) [20]. In the same vein, Ag-decorated Cu-doped ZnO nanoparticles have been successfully fabricated and investigated through XRD and FTIR [21]. Cu-doped ZnO NPs have been used to degrade dyes in the UV-visible region more efficiently as compared with undoped ZnO NPs [22]. Photocatalytic activity of Cu-doped ZnS is found to be significantly higher under visible light as compared with UV light. The optimal concentration of Cu-doped ZnS was observed to be 3 mol% for photocatalytic applications [23]. The photocatalytic activity of Cu-doped ZnS was probed by the hydrogen generation experiment using a solar simulator. The highest apparent quantum yield was ~11% [24]. These copper-doped zinc-related materials have been shown to demonstrate the highest catalytic activity and morphological enhancement as compared with the pristine materials by enhancing the production of free radicals. In this present work, Cu-doped ZnSe nanoparticles were synthesized from a simple co-precipitation method and their catalytic activity was examined by employing methyl orange (MO) dye in aqueous solution as a model dye and its rate of kinetics was investigated. The bacterial efficiency of the Cu-doped ZnSe nanoparticles was examined by employing gram-positive (*S. aureus*) and gram-negative (*E. coli*) bacteria. The photocatalytic and bacterial efficiency of the Cu-doped ZnSe nanoparticles prove it as a promising material for the removal of pollutants in water.

2. Materials and Methods

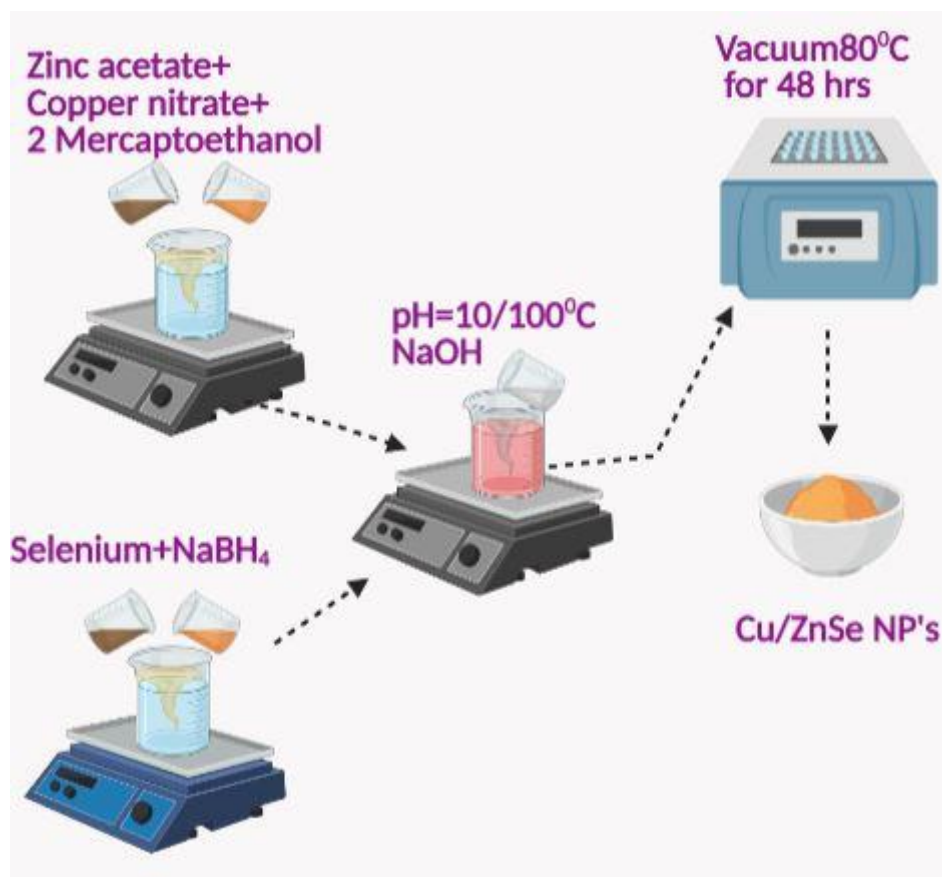
2.1. Materials

The synthesized materials were procured from HiMedia, Mumbai, India (99% purity). The chemicals (copper nitrate, CuNO₃), zinc acetate dihydrate—C₄H₆O₄Zn₂H₂O, 2-mercaptoethanol—C₂H₆OS, sodium borohydride—NaBH₄, methyl orange dye—C₁₄H₁₄N₃NaO₃S, and sodium hydroxide—NaOH were used for further processing of Cu-doped ZnSe nanoparticles. The solvent is a doubly distilled water.

2.2. Synthesis Process

The Cu-doped ZnSe nanoparticles were synthesized by a two-step process. The first step is to dissolve 0.5 M zinc acetate dihydrate solution in 2-mercaptoethanol and 0.01 M copper nitrate solutions by continuously stirring with a magnetic stirrer. Subsequently,

selenium powder (0.5 M) was added with sodium hydroxide solution to obtain the sodium hydroxide selenide solution. The zinc and selenium solution was then heated to 100 °C while maintaining the pH at 10 with NaOH. The reaction mixture was then allowed to stir for 24 h at 100 °C. Thereafter, the obtained precipitate was washed with ethanol or distilled water followed by drying in vacuum for 48 h at 80 °C. Finally, the processed powdered sample was kept in an oven for 200 °C. The as prepared powder sample was then used for further measurements. The same method was used for synthesizing 0.05 M, 0.01, and 0.1 M copper nitrate-doped ZnSe nanoparticles [25]. The synthesis process of Cu-doped ZnSe nanoparticles is depicted in Scheme 1.



Scheme 1. Synthesis steps of the Cu-doped ZnSe nanoparticles.

2.3. Characterization

Crystal structure and the phase changes were probed using X-ray diffraction (PANalytical X-ray diffractometer, Cu- K_{α} wavelength) (JDX-3532, JEOL, Tokyo, Japan). The optical identity was derived from UV/vis DRS (Shimadzu-2700 spectrophotometer). The surface functional groups were observed with an FT-IR spectrometer (Perkin Elmer) (IR Prestige 21, Shimadzu, Kyoto, Japan). The morphological changes were identified by employing FE-SEM with EDX (Sigma, Zeiss, Jena, Germany) and HR-TEM (JEOL-2100) (Sigma, Zeiss, Jena, Germany). Furthermore, the binding energy of the synthesized materials was studied by XPS (XPS, PHI 500, California, CA, USA).

2.4. Antibacterial Activity

The bacterial evaluation of the synthesized Cu-doped ZnSe nanoparticles was analyzed using gram-positive (*S. aureus*) and gram-negative (*E. coli*) bacteria. The disc diffusion method was used to find the efficiency of the nanoparticles. Mueller Hinton broth was used to grow the bacteria overnight. The grown bacteria were isolated ($100 \mu\text{L} \times 10^{-7}$ CFU) and streaked onto the sterilized agar Petri plates. A paper disc was inserted onto the Petri plates

with a diameter of 6 mm. The disc was loaded with various concentrations (25 μL , 50 μL , and 100 μL) of nanoparticles. The weighted discs were incubated for 24 h at 37 °C. The incubated discs were then probed for the zone of inhibition for the cultured bacteria. The zone shows prominent bacterial destruction, where the range of the zone was measured in mm scale [25]. The same experiment conditions were triplicated for accuracy.

2.5. Photocatalytic Dye Degradation

The photocatalytic dye degradation of MO dye was investigated by employing Cu-doped ZnSe nanoparticles. The light source used for the experiment is a Xenon lamp that gives off visible light. The catalyst (10 mg) was dissolved in 100 mL of the dye solution and placed in dark conditions for 30 min. The dark condition helped to achieve the adsorption desorption equilibrium. Then, visible light was irradiated on the sample and, after a certain time interval, an aliquot of 3 mL from the solution was taken out and centrifuged at 5000 rpm to remove the nanoparticles to determine the dye degradation accuracy. The collected samples were recorded in a UV/vis spectrometer. The dye degradation efficiency was calculated using Equation (1) as follows:

$$\text{Degradation efficiency (\%)} = \frac{C_0 - C}{C_0} \times 100 \quad (1)$$

where C_0 denotes initial dye concentration without light and C is the light exposed dye concentration.

3. Results and Discussion

3.1. XRD Analysis

The XRD pattern of copper-doped ZnSe nanoparticles is shown in Figure 1. The copper peaks are indexed at $2\theta = 43.8^\circ$, 50.7° , and 74.3° , corresponding to (111), (200), and (220) miller planes, respectively. Their patterns are well-matched with the std. JCPDS card no. of 04-0836 with an FCC (face-centered cubic) structure [25,26]. The copper modifies the ZnSe nanoparticles, as shown in Figure 1. The ZnSe nanoparticles' peaks were observed at $2\theta = 27.3^\circ$, 45.3° , 53.7° , 66° , and 73° for (111), (220), (311), (400), and (203) planes, respectively. The distinct peaks of copper as introduced into the ZnSe nanoparticles by doping have marginally changed the nature of the ZnSe nanoparticles. By introducing copper into ZnSe, the cubic structure is modified with respect to the size and growth of orientation of the NP, which converts copper to Cu (II) phase. The Cu (II) phase is confirmed by the narrow XRD peaks at 31.7° . The Cu (II) phase was reassured by the XPS technique. The pristine ZnSe nanoparticles are reoriented by the addition of copper into the crystal system. The copper-doped ZnSe nanoparticles' size was determined by the Debye–Sherrer equation. The calculated values are $18 < 24 < 31$ nm for $0.01 < 0.05 < 0.1$ M copper-doped into the ZnSe nanoparticles, respectively [27].

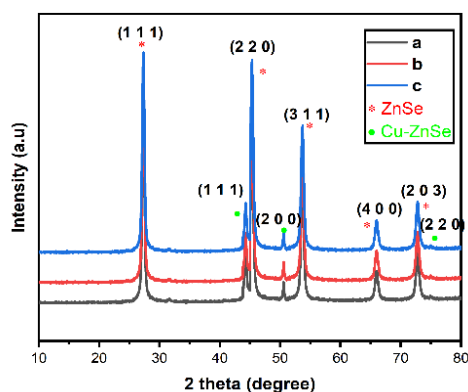


Figure 1. X-ray diffraction patterns of Cu (0.01, 0.05, and 0.1 M)-doped ZnSe nanoparticles.

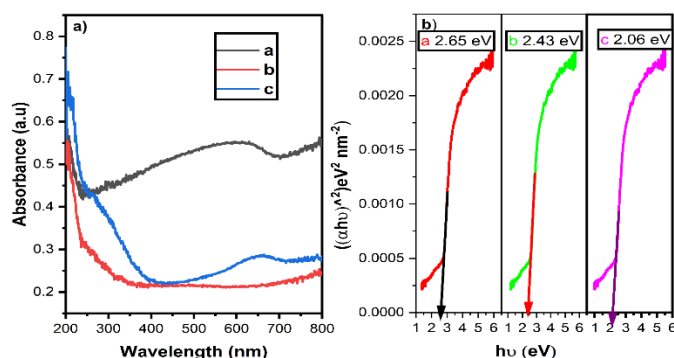


Figure 3. (a) UV/vis DRS spectra of the Cu (0.01, 0.05, and 0.1 M)-doped ZnSe nanoparticles and (b) bandgap spectrum.

3.4. FE-SEM and EDX Analysis

The surface morphology and elemental composition of the synthesized Cu-doped ZnSe nanoparticles were evaluated by field emission scanning electron microscope (FE-SEM) coupled with energy dispersive X-ray analysis (EDX), as shown in Figure 4a–f. The raw ZnSe nanoparticles have been shown to exhibit a spherical shape [32]. The presence of Cu^{2+} ions in the ZnSe surface modifies the shape and size of the Cu-doped ZnSe nanoparticles (Figure 4a–c). The Cu-doped ZnSe nanoparticles exhibit a quasi-spherical shape. The modifications in the structure due to the dopant in various concentration (0.01, 0.05, and 0.1 M of Cu^{2+} ions) induce a structural and morphological stability. The presence of low-level Cu^{2+} in the ZnSe nanoparticles shows a mixed spherical shape (Figure 4a,b). The copper-rich ZnSe nanoparticle shows a better quasi-spherical shape than samples a and b (Figure 4c).

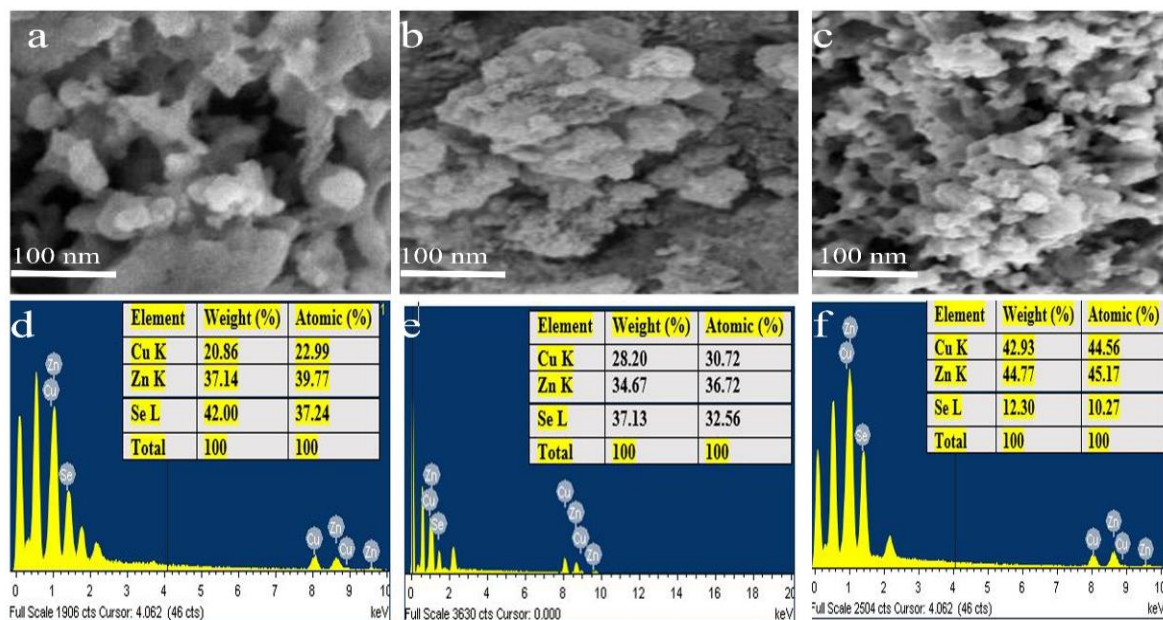


Figure 4. FE-SEM images of Cu (a) 0.01 M at 100 nm, (b) 0.05 M at 100 nm, and (c) 0.1 M at 100 nm-doped ZnSe nanoparticles and EDX spectrum of Cu (d) 0.01 M at 100 nm, (e) 0.05 M at 100 nm, and (f) 0.1 M at 100 nm-doped ZnSe nanoparticles.

The atomic and weight percentages of the elements present in the sample were measured by energy dispersive X-ray analysis (EDX) (Figure 4d–f). The presence of copper, zinc, and selenium confirms the existence of the respective elemental constituents. The elements and their atomic and weight percentages are tabulated in Figure 4d–f as an inset.

The different concentration of Cu^{2+} was listed in the EDX spectrum. The high copper content results in a change in the shape and size of the as synthesized nanoparticles.

3.5. HR-TEM Analysis

The synthesized Cu-doped ZnSe nanoparticles represent the HR-TEM image of quasi-spherical shape in Figure 5a,b. Cu^{2+} ions have similar ionic radii to Zn^{2+} ions in the Cu-doped ZnSe lattice. Therefore, the Cu^{2+} ions are expected to be incorporated into the ZnSe crystal structure. The size of the Cu-doped ZnSe nanoparticle is 33 nm, which is nearly equal to the crystallite size. The poly crystallite nature of the spherical shape informed the formation of the Cu^{2+} and Cu (II) phase in ZnSe nanoparticles. The raw ZnSe nanoparticle has been found to exhibit a spherical shape, but the presence of dopant as Cu reforms the shape into a quasi-spherical shape [25,34].

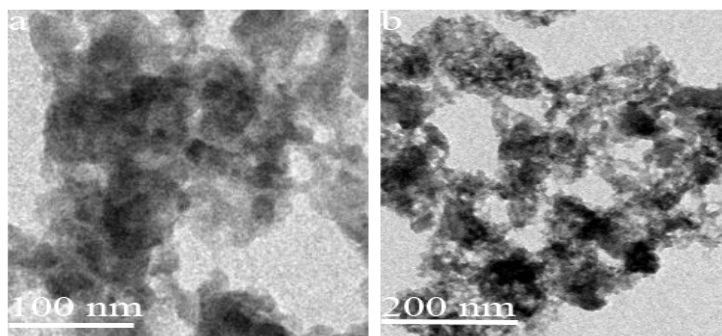


Figure 5. HR-TEM images of Cu (0.1 M)-doped ZnSe nanoparticles (a) 100 nm (b) 200 nm.

3.6. XPS Analysis

The valency and chemical state and bonding between the materials were elucidated by X-ray photoelectron spectroscopy (XPS). Figure 6a–e represent the characteristic spectrum of Cu-doped ZnSe nanoparticles in the survey spectrum (a), Cu-2p spectrum (b), Zn-2p spectrum (c), Se-3d spectrum (d), and C-1s spectrum (e). The Cu 2p_{3/2} (934.58 eV) and Cu 2p_{1/2} (954.58 eV) (Figure 6a) represent the metallic Cu core with the difference of 20 eV (spin-orbit coupling). The remaining two peaks of the copper spectrum indicate the Cu 2p state and represent the existence of the Cu^{2+} with a binding energy of 942.65 eV and 962.65 eV [35]. The peaks at 1022.23 eV and 1045.48 eV in Figure 6b point towards Zn 2p_{1/2} and Zn 2p_{3/2}, respectively (Figure 6c) [36]. The selenium peaks at 59.33 eV and 55.06 eV represent Se-3d_{3/2} and Se 3d_{5/2}, respectively [37]. The copper state of C-1s represents the existence of Cu^{2+} , Zn^{2+} , and Se^{2-} in 285.40 eV (Figure 6e). The metal ions and bonding between them demonstrate the successful preparation of Cu-doped ZnSe nanoparticles. Copper is widely used for photocatalytic applications thanks to its oxidative tendency. The zinc selenide nanoparticles doped with copper metal result in enhancing the catalytic activity used for degradation of the organic dyes and antibacterial activity.

3.7. Antibacterial Activity

The antibacterial activity of Cu-doped ZnSe nanoparticles was investigated by the dose diffusion method against gram-positive (*S. aureus*) and gram-negative (*E. coli*) bacteria. The Cu^{2+} ions increased the zone of inhibition for the target species as the concentration of Cu-doped ZnSe nanoparticles increased from 25 μL to 100 μL . The three different concentrations of Cu-doped ZnSe nanoparticles were used to target the bacterial strains and develop a zone of inhibitions, as shown in Figure 7. The largest zone of inhibition is shown for the highest concentration of Cu. The dissolution rate and release of ions determined the destruction of the strains. Here, the gram-negative bacterial growth was suppressed more than that of gram-positive bacteria. The gram-negative bacteria cell wall is weaker than that of the gram-positive bacteria. Therefore, the Cu^{2+} ions easily enter

and constrict the growth of negative bacteria. Thus, the Cu-doped nanoparticles produce efficient antibacterial activity [38].

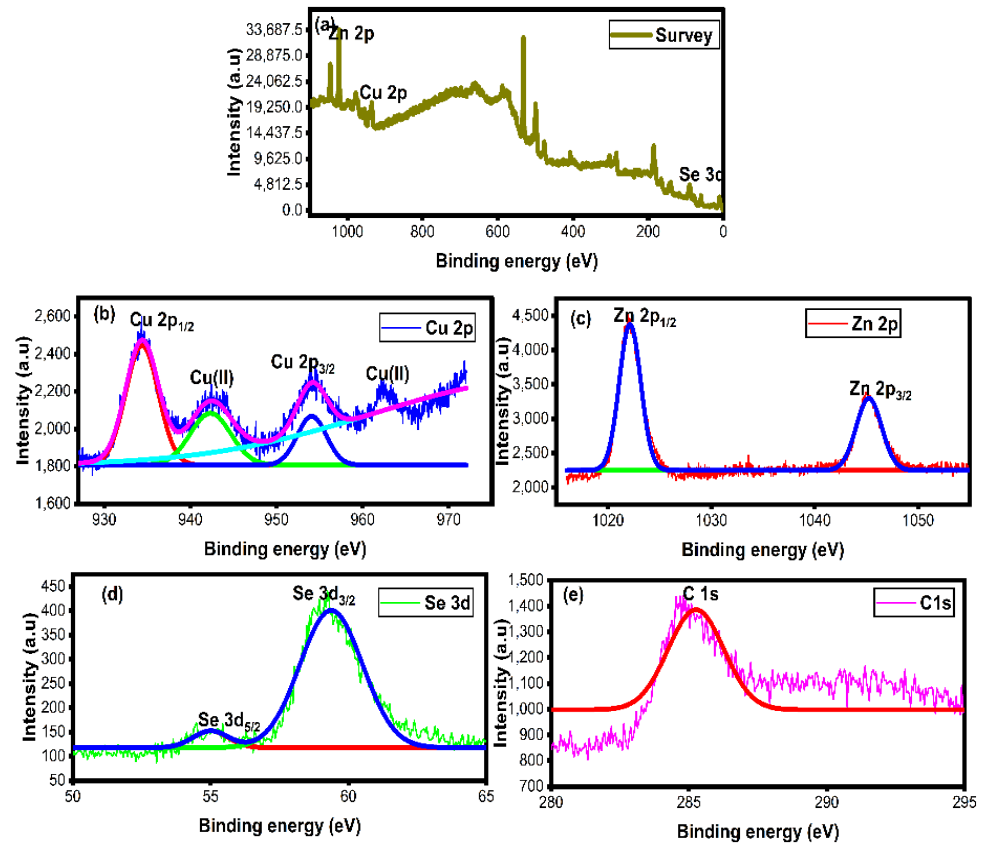


Figure 6. XPS spectra of Cu/ZnSe (0.1 M) nanoparticles: (a) wide spectrum, (b) Cu-2p spectrum, (c) Zn 2p spectrum, (d) Se 3d spectrum, and (e) C 1s spectrum.

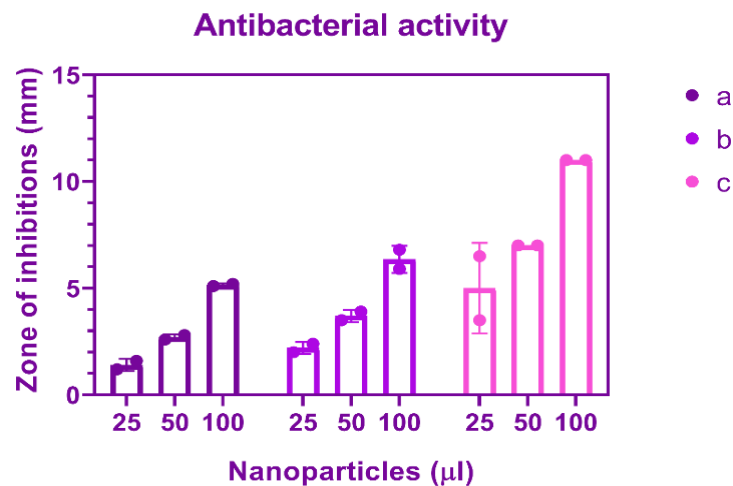


Figure 7. Antibacterial activity of Cu (a) 0.01, (b) 0.05, and (c) 0.1 M doped ZnSe nanoparticles.

3.8. Mechanism of Antibacterial Activity of Cu-Doped ZnSe Nanoparticles

The possible mechanism of Cu-doped ZnSe nanoparticles against bacteria is shown in Figure 8. The mechanism is based on two important actions, which are

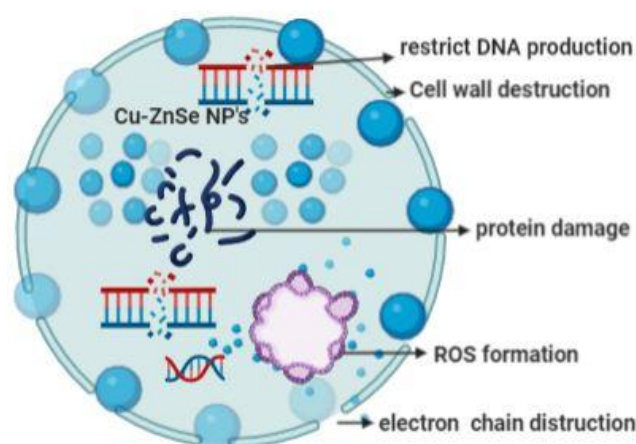


Figure 8. Antibacterial activity mechanism of Cu/ZnSe nanoparticles.

- Cell wall destruction;
- ROS formation (reactive oxygen species).

The positively charged nanoparticles target the negatively charged bacteria, interacting by the electrostatic force of attraction. The interaction results in electron chain destruction, restricts DNA production, and damages the protein. The ROS formation may stop the multiplication/production of the bacteria, which leads to cell death [39].

3.9. Photocatalytic Dye Degradation

The photocatalytic dye degradation of Cu-doped ZnSe nanoparticles was examined against the MO dye under a visible light source using a xenon lamp above 400 nm. The degradation spectrum is shown in Figure 9. The MO dye absorbance decreased with the addition of a catalyst and increased time interval. The degradation activity of pristine ZnSe nanoparticles shows a decrease in absorbance by 75% for MO in 120 min [40]. The dye is slowly shown to lose its colour with increasing time. The presence of copper in Cu-doped ZnSe nanoparticles enhances the surface area and induces photo charge carriers to degrade MO dye, as depicted in Figure 10a,b. The % of photodegradation of the dye is estimated as 78% < 83% < 87% for different concentrations of Cu in ZnSe nanoparticles. The photolysis process without the catalyst shows a meagre value of photodegradation of MO, i.e., 4%. The commercial photocatalyst of P25 as compared with Cu/ZnSe nanoparticles reflects a degradation of 96%, which is nearly equal to the Cu/ZnSe catalyst at 0.1 M Cu concentration. The visible light source was irradiated onto the Cu-doped ZnSe nanoparticles with MO dye in the solution, allowing the electrons to move from a low energy valence band to a high energy conduction band. The charge carriers as electrons and holes render the property of reduction and oxidation in the conduction band and valence band, respectively. The copper metal may improve the surface morphology of ZnSe nanoparticles, which could allow more light penetration to the active sites with a decrease in band gap. The p-type copper-doped ZnSe nanoparticles induce the process of oxidation and reduction process for efficient catalytic activity. The rate of degradation was calculated using the pseudo-first order kinetics and the value of the rate constant is enlisted as follows: $0.01243 \text{ min}^{-1} < 0.01300 \text{ min}^{-1} < 0.1334 \text{ min}^{-1}$. Sample c has higher kinetics values than the other samples (Figure 10b), which shows better performance for photodegradation.

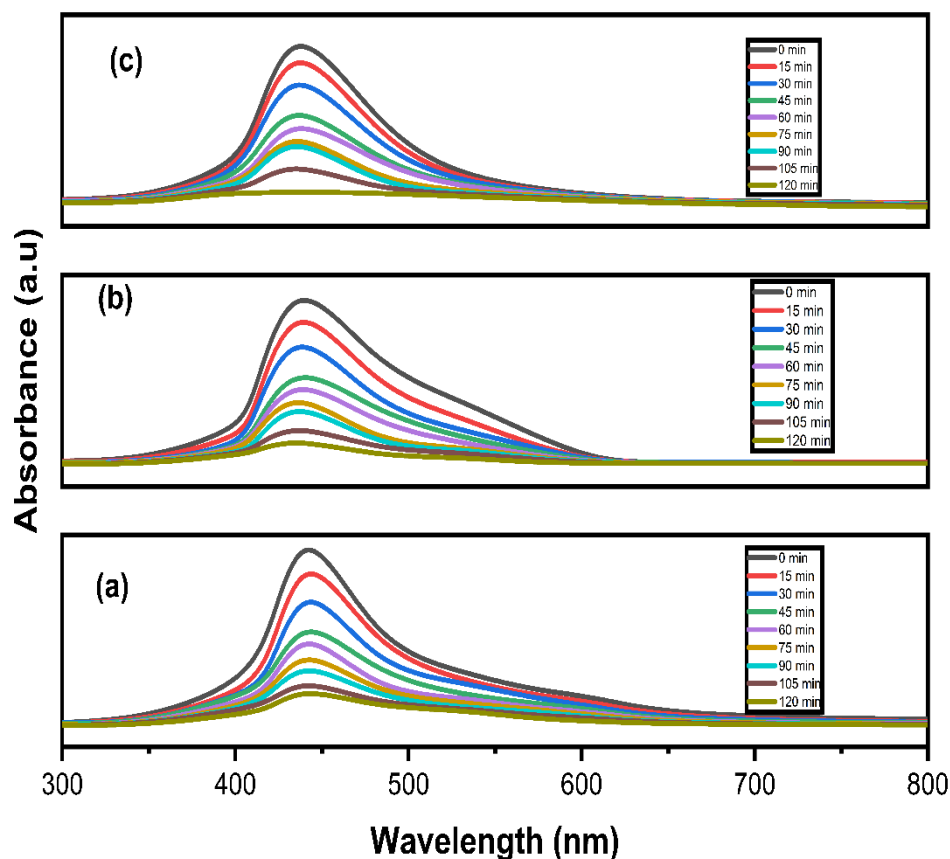


Figure 9. Photocatalyst dye degradation with (a) 0.01 M Cu, (b) 0.05 M Cu, and (c) 0.1 M Cu in Cu/ZnSe nanoparticles against MO dye spectrum.

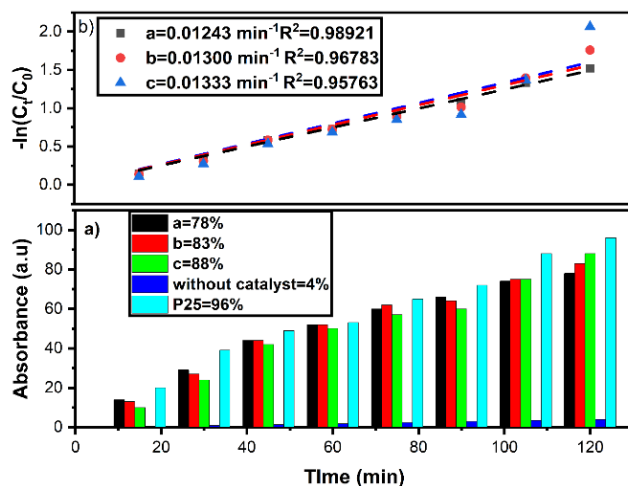


Figure 10. Photocatalytic dye degradation (a) compared with commercial photocatalyst and without catalyst and (b) pseudo-first-order kinetics of the Cu/ZnSe nanoparticles with different Cu concentrations.

4. Conclusions

The facile co-precipitation method was used to synthesize Cu-doped ZnSe nanoparticles. The co-precipitation method has been found to be simple, less time- and energy-consuming, sustainable, and economical compared with other conventional methods. The copper integration was carried out on a ZnSe cubic structure. The structural modifications were confirmed by XRD and the average crystallite size was estimated as 31 nm for 0.1 M

Cu-doped ZnSe. The phase purity, optical transformations, and valency of the Cu-doped ZnSe nanoparticles revealed the structural modification of the catalyst. Different concentrations of Cu-doped ZnSe nanoparticles were used to study the catalytic activity. Among them, 0.1 M Cu-doped ZnSe nanoparticles have exhibited excellent photocatalytic activity towards MO dye. The 0.1 M Cu-doped ZnSe nanoparticles also exhibit noticeable antibacterial activity against the gram-positive and gram-negative bacteria. This work suggests that the Cu-doped ZnSe nanoparticles portray a prominent photocatalytic and antibacterial activity. Hence, the synthesized Cu-doped ZnSe nanoparticles can be used for developing a large-scale wastewater purification system for the degradation of contaminants.

Author Contributions: Conceptualization, V.B. and S.L.R.; methodology, A.A.; software, V.B.; validation, K.M.A., T.S.A. and M.O.; formal analysis, S.A. (S. Ajitha); investigation, F.J.I.; resources, M.O.; data curation, M.O.; writing—original draft preparation, A.A.; writing—review and editing, F.J.I.; visualization, V.B.; supervision, S.A. (Shafaqat Ali); project administration, S.A. (Shafaqat Ali); funding acquisition, T.S.A. All authors have read and agreed to the published version of the manuscript.

Funding: The authors appreciated Taif University Researchers Supporting Project number TURSP-2020/267, Taif University, Taif, Saudi Arabia. This research was funded by the Deanship of Scientific Research at Princess Nourah bint Abdulrahman University through the Fast-track Research Funding Program.

Institutional Review Board Statement: Not applicable.

Informed Consent Statement: Not applicable.

Data Availability Statement: Not applicable.

Conflicts of Interest: The authors declare no conflict of interest.

References

1. Julkapli, N.M.; Bagheri, S.; Bee Abd Hamid, S. Recent Advances in Heterogeneous Photocatalytic Decolorization of Synthetic Dyes. *Sci. World J.* **2014**, *2014*, 692307. [[CrossRef](#)] [[PubMed](#)]
2. Bibi, S.; Ahmad, A.; Anjum, M.A.R.; Haleem, A.; Siddiq, M.; Shah, S.S.; Al Kahtani, A. Photocatalytic degradation of malachite green and methylene blue over reduced graphene oxide (rGO) based metal oxides (rGO-Fe₃O₄/TiO₂) nanocomposite under UV-visible light irradiation. *J. Environ. Chem. Eng.* **2021**, *9*, 105580. [[CrossRef](#)]
3. Ahmad, I.; Jamal, M.A.; Iftikhar, M.; Ahmad, A.; Hussain, S.; Asghar, H.; Saeed, M.; Yousaf, A.B.; Karri, R.R.; Al-kadhi, N.S.; et al. Lanthanum-Zinc Binary Oxide Nanocomposite with Promising Heterogeneous Catalysis Performance for the Active Conversion of 4-Nitrophenol into 4-Aminophenol. *Coatings* **2021**, *11*, 537. [[CrossRef](#)]
4. Kashif, M.; Jafaar, E.; Sahari, S.K.; Low, F.W.; Hoa, N.D.; Ahmad, A.; Abbas, A.; Ngaini, Z.; Shafa, M.; Qurashi, A. Organic sensitization of graphene oxide and reduced graphene oxide thin films for photovoltaic applications. *Int. J. Energy Res.* **2021**, *45*, 9657–9666. [[CrossRef](#)]
5. Saleem, M.; Irfan, M.; Tabassum, S.; Albaqami, M.D.; Javed, M.S.; Hussain, S.; Pervaiz, M.; Ahmad, I.; Ahmad, A.; Zuber, M. Experimental and theoretical study of highly porous lignocellulose assisted metal oxide photoelectrodes for dye-sensitized solar cells. *Arab. J. Chem.* **2021**, *14*, 102937. [[CrossRef](#)]
6. Aravind, M.; Ahmad, A.; Ahmad, I.; Amalanathan, M.; Naseem, K.; Mary, S.M.M.; Parvathiraja, C.; Hussain, S.; Algarni, T.S.; Zuber, M.P.M. Critical green routing synthesis of silver NPs using jasmine flower extract for biological activities and photocatalytic degradation of methylene blue. *J. Environ. Chem. Eng.* **2021**, *9*, 104877. [[CrossRef](#)]
7. Hussain, S.; Khan, A.J.; Arshad, M.; Javed, M.S.; Ahmad, A.; Shah, S.S.A.; Khan, M.R.; Akram, S.; Zulfiqar, Ali, S.; et al. Charge storage in binder-free 2D-hexagonal CoMoO₄ nanosheets as a redox active material for pseudocapacitors. *Ceram. Int.* **2021**, *47*, 8659–8667. [[CrossRef](#)]
8. Beena, V.; Rayar, S.L.; Ajitha, S.; Ahmad, A.; Albaqami, M.D.; Alsabar, F.A.A.; Sillanpää, M. Synthesis and Characterization of Sr-Doped ZnSe Nanoparticles for Catalytic and Biological Activities. *Water* **2021**, *13*, 2189. [[CrossRef](#)]
9. Ahmad, A.; Jini, D.; Aravind, M.; Parvathiraja, C.; Ali, R.; Kiyani, M.Z.; Alothman, A. A novel study on synthesis of egg shell based activated carbon for degradation of methylene blue via photocatalysis. *Arab. J. Chem.* **2020**, *13*, 8717–8722. [[CrossRef](#)]
10. Vaez, Z.; Javanbakht, V. Synthesis, characterization and photocatalytic activity of ZSM-5/ZnO nanocomposite modified by Ag nanoparticles for methyl orange degradation. *J. Photochem. Photobiol. A Chem.* **2020**, *388*, 112064. [[CrossRef](#)]
11. Deng, H.; Zhang, M.; Cao, Y.; Lin, Y. Decolorization of Reactive Black 5 by Mesoporous Al₂O₃@TiO₂ Nanocomposites. *Environ. Prog. Sustain. Energy* **2019**, *38*, S230–S242. [[CrossRef](#)]
12. Rajendran, S.; Khan, M.M.; Gracia, F.; Qin, J.; Gupta, V.K.; Arumainathan, S. Ce³⁺-ion-induced visible-light photocatalytic degradation and electrochemical activity of ZnO/CeO₂ nanocomposite. *Sci. Rep.* **2016**, *6*, 31641. [[CrossRef](#)]

13. Shaikh, A.F.; Arbuj, S.S.; Tamboli, M.S.; Naik, S.D.; Rane, S.B.; Kale, B.B. ZnSe/ZnO nano-heterostructures for enhanced solar light hydrogen generation. *ChemistrySelect* **2017**, *2*, 9174–9180. [[CrossRef](#)]
14. Mkhallid, I.A. Improved photocatalytic performance in Bi₂S₃-ZnSe nanocomposites for hydrogen production. *Ceram. Int.* **2018**, *44*, 22198–22204. [[CrossRef](#)]
15. Ehsan, M.F.; Bashir, S.; Hamid, S.; Zia, A.; Abbas, Y.; Umbreen, K.; Ashiq, M.N.; Shah, A. One-pot facile synthesis of the ZnO/ZnSe heterostructures for efficient photocatalytic degradation of azo dye. *Appl. Surf. Sci.* **2018**, *459*, 194–200. [[CrossRef](#)]
16. Zhang, J.; Tian, P.; Tang, T.; Huang, G.; Zeng, J.; Cui, B.; Shen, Z.; Wang, H.; Kong, Z.; Xi, J.; et al. Excellent photoelectrochemical hydrogen evolution performance of FeSe₂ nanorod/ZnSe 0D/1D heterostructure as efficiency carriers migrate channel. *Int. J. Hydrogen Energy* **2020**, *45*, 8526–8539. [[CrossRef](#)]
17. Sanchez-Martinez, A.; Ortiz-Beas, J.P.; Huerta-Flores, A.M.; López-Mena, E.R.; Pérez-Álvarez, J.; Ceballos-Sanchez, O. ZnSe nanoparticles prepared by coprecipitation method for photocatalytic applications. *Mater. Lett.* **2021**, *282*, 128702. [[CrossRef](#)]
18. Hao, E.; Zhang, H.; Yang, B.; Ren, H.; Shen, J. Preparation of Luminescent Polyelectrolyte/Cu-Doped ZnSe Nanoparticle Multilayer Composite Films. *J. Colloid Interface Sci.* **2001**, *238*, 285–290. [[CrossRef](#)] [[PubMed](#)]
19. Ummartyotin, S.; Bunnak, N.; Juntaro, J.; Sain, M.; Manuspiya, H. Synthesis and luminescence properties of ZnS and metal (Mn, Cu)-doped-ZnS ceramic powder. *Solid State Sci.* **2014**, *14*, 299–304. [[CrossRef](#)]
20. Srivastava, R.K.; Pandey, N.; Mishra, S.K. Effect of Cu concentration on the photoconductivity properties of ZnS nanoparticles synthesized by co-precipitation method. *Mater. Sci. Semicond. Process.* **2013**, *16*, 1659–1664. [[CrossRef](#)]
21. Modwi, A.; Taha, K.K.; Khezami, L.; Boudina, M.; Khairy, M.; Al-Duaij, O.K.; Talab, S. Dependence of the electrical properties of Cu-doped ZnO nanoparticles decorated by Ag atoms. *Z. Phys. Chem.* **2021**, *235*, 745–767. [[CrossRef](#)]
22. Mittal, M.; Sharma, M.; Pandey, O.P. UV-Visible light induced photocatalytic studies of Cu doped ZnO nanoparticles prepared by co-precipitation method. *Sol. Energy* **2014**, *110*, 386–397. [[CrossRef](#)]
23. Chauhan, R.; Kumar, A.; Chaudhary, R.P. Photocatalytic degradation of methylene blue with Cu doped ZnS nanoparticles. *J. Lumin.* **2014**, *145*, 6–12. [[CrossRef](#)]
24. Senda, S.; Arai, T.; Sato, Y.; Shinoda, K.; Jeyadevan, B.; Tohji, K. Influence of Cu on the photocatalytic activity of ZnS nanoparticles. *AIP Conf. Proc.* **2006**, *833*, 65. [[CrossRef](#)]
25. Beena, V.; Ajitha, S.; Rayar, L.S.; Parvathiraja, C.; Kannan, K.; Palani, G. Enhanced Photocatalytic and Antibacterial Activities of ZnSe Nanoparticles. *J. Inorg. Organomet. Polym. Mater.* **2021**, *6*, 1–12.
26. Bezverkhyy, I.; Skrzypski, J.; Safonova, O.; Bellat, J.P. Sulfidation mechanism of pure and Cu-doped ZnO nanoparticles at moderate temperature: TEM and in situ XRD studies. *J. Phys. Chem. C* **2012**, *116*, 14423–14430. [[CrossRef](#)]
27. Hao, H.; Yao, X.; Wang, M. Preparation and optical characteristics of ZnSe nanocrystals doped glass by sol–gel in situ crystallization method. *Opt. Mater.* **2007**, *29*, 573–577. [[CrossRef](#)]
28. Eren, E.; Afsin, B. An investigation of Cu (II) adsorption by raw and acid-activated bentonite: A combined potentiometric, thermodynamic, XRD, IR, DTA study. *J. Hazard. Mater.* **2008**, *151*, 682–691. [[CrossRef](#)]
29. Chen, R.; Guo, C.; Chu, W.; Jiang, N.; Li, H. ATR-FTIR study of Bacillus sp. and Escherichia coli settlements on the bare and Al₂O₃ coated ZnSe internal reflection element. *Chin. Chem. Lett.* **2019**, *30*, 115–119. [[CrossRef](#)]
30. Majumdar, S.S.; Das, S.K.; Saha, T.; Panda, G.C.; Bandyopadhyay, T.; Guha, A.K. Adsorption behavior of copper ions on Mucor rouxii biomass through microscopic and FTIR analysis. *Colloids Surf. B Biointerfaces* **2008**, *63*, 138–145. [[CrossRef](#)]
31. Hines, M.A.; Guyot-Sionnest, P. Bright UV-blue luminescent colloidal ZnSe nanocrystals. *J. Phys. Chem. B.* **1998**, *102*, 3655–3657. [[CrossRef](#)]
32. Giordano, F.; Vennestrøm, P.N.; Lundegaard, L.F.; Stappen, F.N.; Mossin, S.; Beato, P.; Bordiga, S.; Lamberti, C. Characterization of Cu-exchanged SSZ-13: A comparative FTIR, UV-Vis, and EPR study with Cu-ZSM-5 and Cu-β with similar Si/Al and Cu/Al ratios. *Dalton Trans.* **2013**, *42*, 12741–12761. [[CrossRef](#)]
33. Mallem, S.P.R.; Koduru, M.; Chandrasekhar, K.; Prabhakar Vattikuti, S.V.; Manne, R.; Reddy, V.R.; Lee, J.H. Potato Chip-Like 0d Interconnected ZnCo₂O₄ Nanoparticles High-Perform. Supercapacitors. *Crystals* **2021**, *11*, 469. [[CrossRef](#)]
34. Shakir, M.; Kushwaha, S.K.; Maurya, K.K.; Bhagavannarayana, G.; Wahab, M.A. Characterization of ZnSe nanoparticles synthesized by microwave heating process. *Solid State Commun.* **2009**, *149*, 2047–2049. [[CrossRef](#)]
35. Liang, Q.; Bai, Y.; Han, L.; Deng, X.; Wu, X.; Wang, Z.; Liu, X.; Meng, J. Hydrothermal synthesis of ZnSe: Cu quantum dots and their luminescent mechanism study by first-principles. *J. Lumin.* **2013**, *143*, 185–192. [[CrossRef](#)]
36. Ghodselahe, T.; Vesaghi, M.A.; Shafiekhani, A.; Baghizadeh, A.; Lameii, M. XPS study of the Cu@ Cu₂O core-shell nanoparticles. *Appl. Surf. Sci.* **2008**, *255*, 2730–2734. [[CrossRef](#)]
37. Feliu, S., Jr.; Barranco, V.X.P.S. XPS study of the surface chemistry of conventional hot-dip galvanised pure Zn, galvanneal and Zn–Al alloy coatings on steel. *Acta Mater.* **2003**, *51*, 5413–5424. [[CrossRef](#)]
38. Agostinelli, E.; Battistoni, C.; Fiorani, D.; Mattogno, G.; Nogues, M. An XPS study of the electronic structure of the Zn_xCd_{1-x}Cr₂ (X = S, Se) spinel system. *J. Phys. Chem. Solids* **1989**, *50*, 269–272. [[CrossRef](#)]
39. Nigussie, G.Y.; Tesfamariam, G.M.; Tegegne, B.M.; Weldemichel, Y.A.; Gebreab, T.W.; Gebrehiwot, D.G.; Gebremichel, G.E. Antibacterial activity of Ag-doped TiO₂ and Ag-doped ZnO nanoparticles. *Int. J. Photoenergy* **2018**, *2018*, 5927485. [[CrossRef](#)]
40. Chaliha, C.; Nath, B.K.; Verma, P.K.; Kalita, E. Synthesis of functionalized Cu: ZnS nanosystems and its antibacterial potential. *Arab. J. Chem.* **2019**, *12*, 515–524. [[CrossRef](#)]